Biogeosciences Discuss., https://doi.org/10.5194/bg-2019-53
Manuscript under review for journal Biogeosciences
Discussion started: 18 February 2019

Biogeosciences Discussions Open Access EGU

The influence of reservoir traits on carbon dioxide emissions in the Belo Monte hydropower complex, Xingu River, Amazon – Brazil

Kleiton R. Araújo[1*], Henrique O. Sawakuchi[2-3], Dailson J. Bertassoli Jr.[4], André O. Sawakuchi[1,4], Karina D. da Silva[1,5], Thiago V. Bernardi[1,5], Nicholas D. Ward[6-7], Tatiana S. Pereira[1,5].

[1]Programa de Pós Graduação em Biodiversidade e Conservação, Universidade Federal do Pará, Altamira, 68372 – 040, Brazil,
[2]Centro de Energia Nuclear na Agricultura, Universidade de São Paulo, Piracicaba, Brazil,
[3]Department of Ecology and Environmental Science, Umeå University, Umeå, SE-901 87, Sweden,
[4]Instituto de Geociências, Universidade de São Paulo, São Paulo, Brazil,
[5]Faculdade de Ciências Biológicas, Universidade Federal do Pará, Altamira, 68372 – 040, Brazil,
[6]Marine Sciences Laboratory, Pacific Northwest National Laboratory, Sequim, Washington, 98382, USA,
[7]School of Oceanography, University of Washington, Seattle, Washington, 98195-5351, USA.

**Correspondence to:* Kleiton R. Araújo (kleitonrabelo@rocketmail.com)

Keywords: run-of-the-river reservoir; greenhouse gas emission; tropical river damming.

Biogeosciences Discuss., https://doi.org/10.5194/bg-2019-53
Manuscript under review for journal Biogeosciences
Discussion started: 18 February 2019

Abstract

River damming alters local hydrology, which influences aspects of the carbon cycle such as carbon dioxide (CO_2) production and emissions. Run-of-the-river reservoirs (RORs) are designed to have a smaller flooded area than traditional storage reservoirs, maintaining a river flow similar to natural seasonal water level fluctuation. These features may potentially reduce the impacts of the dam on the natural carbon cycle. However, little information on the influence of RORs on the carbon cycle is available, especially for the Amazon or other large tropical rivers. The Belo Monte hydropower complex is a large ROR located in the Xingu River, a clearwater tributary of the Amazon River. It is composed of two reservoirs; the Xingu Reservoir (XR) with ROR characteristics and the Intermediate Reservoir (IR) with storage reservoir traits. Here we evaluate spatiotemporal variation of surface water CO_2 partial pressure (pCO_2), CO_2 fluxes (FCO_2), and gas exchange coefficients (k_{600}) during the first two years after the impoundment of the Xingu River. Seasonal changes in the water level had a significant influence on pCO_2 with the highest average values observed during high water. The FCO_2 was more variable, although correlated with pCO_2, throughout the two first years of river impoundment. Spatial heterogeneity was observed for pCO_2 during both seasons while FCO_2 showed significant spatial heterogeneity only during the high water period. High water FCO_2 and pCO_2 values were on the same order of magnitude as emissions measured in Amazonian clearwater rivers unaffected by impoundment, but low water values were an order of magnitude higher than previous observations in clearwater rivers with natural flowing waters. Finally, we observed variability in CO_2 fluxes related to the type of environment (i.e., river channel, downstream the dams, outside reservoirs and flooded areas), among reservoirs and the land use of flooded areas after impoundment of the Belo Monte hydropower complex. For example, CO_2 emissions were 15% and 90% higher for the IR compared to XR during high and low water season, respectively, indicating that storage reservoirs may be larger sources of CO_2 to the atmosphere compared to RORs. Since many reservoirs are still planned to be constructed in the Amazon and throughout the world, it is critical to evaluate the implications of reservoir traits on CO_2 fluxes over their entire life cycle in order to generate energy that has lower emissions per KW.

1 Introduction

Rivers and streams are no longer considered passive pipes where terrestrial organic matter (OM) travels unchanged from land to sea (Cole et al., 2007). The OM transported by inland waters may be converted to carbon dioxide (CO_2) or methane (CH_4) and escape to the atmosphere as gaseous emissions (Battin et al., 2009; Ward et al., 2013). Inland waters cover an area of approximately 624,000 km² (about 0.47% of the Earth's land surface) and emit about 1.8 to 3.8 Pg C annually (Abril et al. 2014; Drake et al., 2018; Raymond et al., 2013; Sawakuchi et al., 2017). Despite the relatively small area covered by inland waters, their carbon emissions offset the oceans carbon sink (1.42 ± 0.53 Pg C y^{-1}) (Landchützer et al., 2014).

Channel impoundment promotes several changes on river properties such as water discharge, organic and inorganic sediment input, water temperature, water turbulence and wind shear (St. Louis et al., 2000). These changes alter the microbial community structure and biogeochemical processes in the water column and riverbed sediments, with consequent impacts on the dissolved carbon load, production, and eventual release to the atmosphere as CO_2 (Battin et al., 2008). The intense decomposition of OM contained in flooded soils, in addition to autochthonous OM deposited in the reservoir may lead to an increase of the CO_2 production, leading to higher CO_2 outgassing, particularly during the first years of channel impoundment (Guérin et al., 2006). Reduced water turbidity and elevated light penetration depth due to the increase in water residence time, on the other hand, may counterbalance those emissions due to higher CO_2 uptake by primary producers (Duarte and Prairie, 2005), or alternatively stimulate OM decomposition via photo-oxidation and/or microbial priming effects (Ward et al., 2016).

In order to minimize some of the impacts usually associated with hydropower dams, run-of-the-river (ROR) hydroelectric systems have smaller reservoirs and they operate with seasonal variations in water levels (Csiki and Rhoads, 2010; Egré and Milewski, 2002). The Belo Monte hydroelectric complex in the lower Xingu River operates as a ROR and it is the largest hydropower plant in the Amazon. It ranks third in the world in terms of installed capacity (11,233 MW), but with high variation in energy production throughout the year due to the high seasonality of the water discharge of the Xingu River (Brasil, 2009c). The Xingu River, as other Amazonian clearwater rivers, presents relatively high emissions of CO_2 in natural conditions (pre–impoundment) compared to blackwater or whitewater Amazonian rivers (Sawakuchi et al., 2017). As such, alterations in the natural carbon cycling in this environment may result in direct and significant impacts on the regional carbon budget.

Little information is available for greenhouse gas (GHG) emissions from RORs and the available estimates were mainly obtained through modeling for tropical reservoirs or measurements in small temperate reservoirs (DelSontro et al., 2016; Faria et al., 2015). Hundreds of new hydroelectric reservoirs are currently under construction or planned to be built in the tropical South America, Africa, and Asia, and many of them may be ROR reservoirs (Winemiller et al., 2016). Also, most of the GHG emissions estimates available in the literature are from old reservoirs (Barros et al, 2011; Deemer et al., 2016) and newly flooded reservoirs are still poorly studied. Given that CO_2 emissions during the first years of impoundment are critical to determine the overall carbon balance of a ROR reservoir and to evaluate the carbon intensity of hydroelectricity produced from tropical rivers, assessments of GHG emissions in the early stage of flooding are especially important. As such, this study aims to evaluate the spatial and temporal variation of CO_2 partial pressure (pCO_2) and CO_2 emission and its relevance for GHG fluxes during the first two years after development of the reservoirs of the Belo Monte Hydropower complex in eastern Amazon.

Biogeosciences Discuss., https://doi.org/10.5194/bg-2019-53
Manuscript under review for journal Biogeosciences
Discussion started: 18 February 2019

2 Material and methods

2.1 Study area

The Xingu River is the second largest clearwater tributary of the Amazon River. It drains an area of 504,000 km^2 and flows from central Brazil (15°S) to the lower Amazon River in eastern Amazonia (3°S) (Latrubesse et al., 2005; Brasil, 2009a). It is classified as a clear water river, characterized by neutral to slightly alkaline pH, and low concentration of suspended sediment, with high light penetration (Sioli, 1984). The climate of the region has high seasonality. The rainy period usually starts in December extending until May, with rainfall peaking in March and April (Inmet, 2017). The dry season occurs from June to November, with the driest months being September and October (Fig.1). The average monthly rainfall and temperature were 188 ± 145 mm and 27.5 ± 1.01 °C, respectively (10 year average from 2004 to 2014) (Inmet, 2017). According to the rainfall regime, river discharge is marked by strong seasonality with the low water season occurring from September to November, and the high water season from March to May. The historic average discharge of the Xingu River for the period from 2004 to 2014 was 1,408 ± 513 m^3 s^{-1} for the low water season and 18,983 ± 9,228 m^3 s^{-1} in the high water season (Fig.1). The dominant land cover in the middle and lower Xingu watershed is tropical rainforest, although agriculture and deforested areas occur mainly in the south and southwest of the basin and close to Altamira, the largest city near the Belo Monte hydropower complex (Brasil, 2009a).

The studied area ranges from the lower Iriri River, the largest tributary of the Xingu River, to downstream of the sector known as "*Volta Grande do Xingu"* (Xingu Great Bend), nearby the Vitória do Xingu Municipality (Fig. 2). The Belo Monte hydroelectric complex is classified as a ROR reservoir by Eletrobrás (Brazilian energy company) due the reduced reservoir size, lack of water level control in the main power house, short water residence time and seasonal variation of water discharge (Brasil, 2009b; 2009c). However, the Belo Monte hydroelectric complex is a combination of two reservoirs, one in the river channel that can be considered as a ROR reservoir (although it has spillways, the diminished flooded area still resembles the natural river channel) and another one that operates as an storage reservoir fed with water diverted from the first reservoir. Reservoirs residence time (RT) data was based on Eletrobrás (2009b) and calculations on Faria et al. (2015) supplement material.

The upstream reservoir known as the "Xingu reservoir" (XR) is formed by the impoundment of the Xingu River channel by the Pimental dam (Fig.2), which hosts 6 turbines and floodgates that maintain the water flow upstream. The Xingu reservoir mainly inundated seasonally flooded forest (*igapó*) in islands and at the channel margins, however the relatively reduced flooded area kept the boundaries of the river channel similar to its natural state in the high water season (Fig.2). In addition XR is a reservoir with low RT (0.33 days). Considering these characteristics, the Xingu reservoir will be denominated a ROR.

On ROR projects it is common to construct an associated storage reservoir to optimize the energy production (Egré and Milewski, 2002). The waters of the XR are diverted to feed the second reservoir naturally disconnected from the Xingu River channel, called the "Intermediate reservoir" (IR) (Brasil, 2009b; 2009c). The IR flooded large areas of pasture and upland non-flooded forest ("*terra firme* forest"). It is impounded by the Belo Monte dam, with a powerhouse that hosts 18 turbines comprising 97% of the installed capacity of the Belo Monte hydropower complex (Fig.2). Different from the Pimental dam there is no water flow regulation system in the Belo Monte dam. In comparison to XR, IR has longer RT (1.57 days). Since its characteristics resemble storage reservoirs, the IR will be denominated a storage reservoir.

Both dams have similar intake depth at about 15-20 m (above the hypolimnion) and occupy together an area of 516 km². Approximately 267 km^2 of the reservoirs area correspond to flooded lands and the remaining area is the original river channel during the high water season (Brasil, 2014). The water from the intermediate reservoir returns to the Xingu river channel after flowing around 34 km over flooded lands (Fig.2) (Brasil, 2009b; 2009c). With the deviation of the Xingu River the sector between the two dams, including part of the Xingu Great Bend, had significantly decreased its water discharge. The expected installed power capacity of both reservoirs is 11,233 MW, which is equivalent to 25.4 km²/MW (Brasil, 2009b; 2009c).

2.2 Carbon dioxide partial pressure (pCO_2) and CO_2 fluxes (FCO_2) from the water

The gas sampling survey (Fig.2 and Table 1) occurred during the high water level season in April 2016, May 2017 and during the low water level season in September 2017. Due to technical challenges, pCO_2 data was only collected during 2017 and 2017 FCO_2 samplings were made with different equipment (details below). In order to cover zones with different flooded substrates and hydrologic characteristics, the sampling sites included the original river channel within the XR, flooded lands (forest and pasture) of both reservoirs, upstream and downstream river channel zones outside the influence of the XR and IR, including sites in the lower Iriri River (Fig.2). The sampling sites to measure pCO_2 were separated into three classes (Table 1) according to water depth: (I) near bottom: 0.5-1.0 m above the sediment interface; (II) 60%: at 60% of total water depth; (III) surface: up to 0.3 m of water depth. Four classes were created for FCO_2 estimation, with the purpose of evaluating spatial heterogeneity: (I) outside reservoirs: sites located on the channels of the Xingu and Iriri rivers outside reservoir areas, in sectors upstream and further downstream of the reservoirs; (II) main channel: Xingu River main channel within the reservoir area (XR); (III) flooded areas: lands of pasture and upland forest formerly non-flooded during the high water level season and seasonally-flooded forested islands permanently inundated by the reservoirs; (IV) downstream of the dams: sites immediately downstream of the dams that receive the water discharge from turbines of the XR and IR dams. Sampling sites near the confluence of the Xingu and Iriri Rivers (sites P1 and P3, Table 1) were used as reference sites for areas without direct influence of the reservoirs. The sites further downstream of the dams (P20 and P21) were characterized to investigate the influence of the reservoirs on the downstream FCO_2 (Table 1).

During the year of 2017, high and low water level seasons, values of pCO_2 in the water column were obtained using the headspace equilibration method accordingly to Hesslein et al. (1991). Each site was sampled in triplicates at surface, 60% and near bottom water depths. Polycarbonate bottles of 1 L were overflowed up to three times their volume with water drawn by a submersible pump. Rubber stoppers sealed each bottle and then 60 mL of atmospheric air was injected simultaneously to the withdrawal of the same volume of water creating the headspace. The bottles were shaken for three minutes to equilibrate the gas in the water and headspace air. Water was then re-injected simultaneously to the collection of the headspace air. Atmospheric air samples (60 ml) were also collected and used for corrections considering the concentration of CO_2 in the atmosphere near the water surface of each sampling site. All gas samples were transferred to evacuated glass vials capped with butyl rubber stoppers and sealed with aluminum crimps for laboratory analyses. The pCO_2 data was determined using a Picarro® G2201-i cavity ring-down spectroscopy (CRDS) and calculations were based on Wiesenburg and Guinasso (1979).

Carbon dioxide fluxes from the water to the atmosphere were calculated using an infrared gas analyzer (IRGA) LI-COR® Li820 during 2016 and 2017 high water seasons. The FCO_2 measurements were done using a 7.7 L floating chamber coupled to the IRGA. The analyzer captures the change in CO_2 concentration inside the

chamber by constant recirculation driven by a micro-pump with an air flow of 150 mL min^{-1}. For each site, three consecutive deployments were made for five minutes each from a drifting boat to avoid extra turbulence. During the 2017 low water season, CO_2 mini-loggers (Bastviken et al., 2015) placed inside 6 L floating chambers were used to measure CO_2 fluxes. Sensors were placed inside the 2 chambers and deployed simultaneously during 20-30 minutes with a logging time of 30 seconds. CO_2 fluxes from water to atmosphere were done according to the eq. (1) (Frankignoulle et al. 1998):

$$FCO_2 = \left(\frac{\delta pCO_2}{\delta t}\right)\left(\frac{V}{RT_K A}\right), \quad (1)$$

The CO_2 flux (FCO_2) in mol CO_2 m^{-2} s^{-1} is given by the changes in pCO_2 inside the chamber during the deployment time ($\delta pCO_2/\delta t$, µatm s^{-1}), taking into account the chamber volume (V, m^3), the universal gas constant (R, atm m^3 mol^{-1} K^{-1}), water temperature (T, K) and the area covered by the chamber (A, m^2). Measurements were discarded when the R^2 of the linear relation between pCO_2 and time ($\delta pCO_2/\delta t$) were lower than 0.90 ($R^2 < 0.90$) or the same sampling site had negative FCO_2 values with surface pCO_2 higher than 380 ppm.

2.3 Gas transfer velocity (k_{600})

The air-water gas transfer coefficient k (cm h^{-1}) of CO_2 was estimated based on the flux measurements in association with the surface water concentration by eq. (2):

$$k = \frac{V}{A.\alpha}\ln\left(\frac{pCO_{2w} - pCO_{2i}}{pCO_{2w} - pCO_{2f}}\right)/(t_f - ti), \quad (2)$$

Where V and A are the chamber volume (cm^3) and area (cm^2), α is the Ostwald solubility coefficient (dimensionless), t is the time (h), and the subscripts w, i and f refers to the partial pressure in the surface water, and initial and final time inside the chamber. Ostwald solubility coefficient was calculated from K0 as described by Wanninkhof (2009). To an adequate comparing the k values were normalized into k_{600} – values following the eq. (3) and (4) (Alin et al., 2011; Jähne et al., 1987; Wanninkhof, 1992):

$$k_{600} = k_T\left(\frac{600}{Sc_T}\right)^{-0.5}, \quad (3)$$

Where k_T is the measured k value at in situ temperature (T), Sc_T is the Schmidt number calculated from temperature and 600 is the Schmidt number for temperature of 20° C. The Schmidt number is calculated as a temperature (T) function:

$$Sc_T = 1911.1 - 118.11\,T + 3.4527\,T^2 - 0.041320\,T^3, \quad (4)$$

Gas transfer velocity calculation is related only to 2017 period due methodological issues.

2.4 Physical-chemical characteristics of the water column

Water temperature, water depth, pH, dissolved oxygen (DO) and conductivity measurements were carried out using a multiparameter probe (EXO2®, YSI). These measurements were done following the same water depth classes applied to pCO_2 (surface, 60% and near bottom), during the 2016 and 2017 samplings. Technical challenges prevented measurement of these parameters, other than wind speed, air and water temperatures

during the 2017 low water sampling. Additionally, air temperature and wind speed were measured at the same time of chamber deployments with assistance of a handheld meteorological station (Kestrel® 5500), 2 m above the water surface.

2.5. Statistical analysis

Statistical analyses were performed in order to evaluate the spatial and seasonal variation of FCO_2, pCO_2 and k_{600} variables as well as to check the correlation among CO_2 variables and water column variables. Normality and heterogeneity of variance was not achieved by Shapiro-Wilks and Bartlett tests, respectively. Thus, non-parametric and multivariate statistical tests were used. The seasonal and spatial variability of FCO_2, pCO_2 and k_{600} were tested by PERMANOVA analysis (Anderson, 2001) using the Euclidian index as distance method. The FCO_2 statistics were assessed separately by season due to the different sampling methods. To evaluate the correlation between FCO_2 *versus* pCO_2, FCO_2 *versus* wind speed, k_{600} *versus* wind speed and pCO_2 *versus* physical-chemical variables (pH, DO and water temperature) a Spearman correlation test was performed (Zar, 2010). Lastly, the pCO_2 averages among the reservoirs were tested by a T-test to independent samples, since the assumptions were achieved (Zar, 2010). All statistical analyses were performed in R (R Development Team Core, 2016) using the Vegan package (Oksanen et al., 2017) and Statistica (Statsoft 8.0) using 5% (0.05) as critical alpha for significance.

3 Results

3.1 Temporal and spatial variability in pCO_2 and FCO_2

Our overall pCO_2 results (1163 ± 660 µatm) presented a significant variation between seasons ($F_{2:57}$= 0.76, R^2= 0.01, $p < 0.05$). The pCO_2 averages by season ranged from 976 ± 633 to 1,391 ± 630 µatm for low and high water seasons, respectively (Figure 3). pCO_2 seasonal variability was also evident within the river channel (averaging 789 ± 140 and 675 ± 510 µatm for high and low water, respectively) and flooded areas (averaging 1,774 ± 532 and 1,438 ± 682, for high and low water, respectively). Significant overall pCO_2 variability was also observed among environments ($F_{2:57}$= 14.46, R^2= 0.37, $p < 0.05$), with highest pCO_2 values observed during high water in flooded areas and lowest values occurring in the river channel during low water (Fig.3).

The pCO_2 spatial variability was persistent when seasons were tested separately ($F_{2:24}$= 12.00, R^2= 0.60, $p < 0.05$ for high water season and $F_{2:26}$= 6.35, R^2= 0.36, $p < 0.05$ for low water season). Highest average pCO_2 by environment was observed during the high water season downstream of the dams (1,879 ± 551 µatm) while the river channel showed the lowest (789 ± 140 µatm). In contrast, during the low water season the highest average pCO_2 values were found in flooded areas (1,438 ± 682 µatm). However, outside reservoir areas had the lowest pCO_2 (637 ± 320 µatm) during low water (Fig.3).

Water depth also influenced pCO_2, considering data from both seasons ($F_{2:57}$= 4.58, R^2= 0.07, $p < 0.05$). Higher pCO_2 was registered in near bottom zones in relation to the water surface, averaging 1,269 ± 689 and 998 ± 613 µatm, respectively. The highest and lowest pCO_2 averages were observed near the bottom and 60 % water depths in zones of flooded areas and river channel (averaging 2,838 ± 83.19 and 281 ± 143 µatm, respectively) (Table 2).

Significant fluctuation of pCO_2 can be observed according to water season and type of sampling site, as described previously, with these variations influencing FCO_2 values. As such, pCO_2 was positively correlated to

FCO_2 during both high and low water (r= 0.80; $p < 0.05$ and r= 0.68; $p < 0.05$, respectively) (Fig.3). The average FCO_2 for all sites during 2016 and 2017 high water seasons was 1.38 ± 1.12 µmol CO_2 m^{-2} s^{-1}, without significant variation between years ($F_{1:28}$= 0.09, R^2= 0.01, $p > 0.05$). Due to the lack of variation between high water FCO_2 in both years, these data were treated as a single data set for the later calculations. As previously mentioned, the different sensors used to measure the FCO_2 in the low water season of 2017 could not be cross-calibrated with the IRGA used for the flux measurements during the two high water sampling campaigns, therefore we choose to evaluate the spatial variation separately, without a seasonal comparison for FCO_2.

The highest and lowest FCO_2 values were observed during the low water season (12.00 ± 3.21 µmol CO_2 m^{-2} s^{-1} and -0.52 µmol CO_2 m^{-2} s^{-1}) (Fig.3). Significant FCO_2 variation between environments sampled during high water was observed ($F_{3:28}$= 7.94, R^2= 0.43, $p < 0.05$), otherwise the low water season had relatively homogeneous FCO_2 values ($F_{3:17}$= 2.67, R^2= 0.14, $p > 0.05$) (Fig.4). The highest and lowest average FCO_2 occurred during the high water season in sectors downstream of the dams (2.89 ± 1.74 µmol CO_2 m^{-2} s^{-1}) and on flooded areas (0.84 ± 0.42 µmol CO_2 m^{-2} s^{-1}, both reservoirs), respectively. Negative fluxes of CO_2 were observed during the low water season in the river channel exclusively in areas outside the reservoirs (Table 2) (Fig.4)

Similarly to pCO_2, the fluxes in the river channel were higher in the high water season, while on flooded areas it was lower during this season (Table 2).

3.2 Run-of-the-River and Storage reservoirs

A pronounced decrease in average pCO_2 values was observed from high water to low water season in the XR (1,244 ± 698 and 839 ± 646 µatm, respectively), while the opposite occurred on the IR (1,676 ± 323 and 1,797 ± 354 µatm, respectively). FCO_2 followed the same pattern in both reservoirs, with a decrease in average values in XR from high water (0.94 ± 0.41 µmol CO_2 m^{-2} s^{-1}) to low water seasons (0.69 ± 0.28 µmol CO_2 m^{-2} s^{-1}) and an FCO_2 increase in the IR from high water (1.08 ± 0.62) to low water seasons (7.32 ± 4.06 µmol CO_2 m^{-2} s^{-1}).

Spatial analyses compared the distribution of pCO_2, FCO_2, k_{600} and wind velocities within and between both reservoirs. For this analysis, flooded areas and river channel on XR were evaluated together as well as downstream the dams and outside reservoirs. pCO_2 showed no significant difference between the XR and the IR ($F_{2:57}$= 0.76, R^2= 0.01, $p > 0.05$), even when seasons were evaluated separately ($F_{1:24}$= 1.12, R^2= 0.01, $p > 0.05$ and $F_{2:32}$= 0.99, R^2= 0.03, $p > 0.05$ to high and low water, respectively). However, when both reservoirs were compared, XR presented pCO_2 on average 721 µatm lower (T-value= -3.31, df= 39, $p < 0.05$). Standing vegetation type in XR flooded areas influenced pCO_2. Different pCO_2 values were observed for pasture (1,161 and 708 ± 260 µatm, for high and low water, respectively), upland forest (1,750 ± 157 and 874 ± 153 µatm, for high and low water, respectively) and seasonally flooded forest (1,189 ± 38 and 880 ± 46 µatm, to high and low water respectively). As expected, FCO_2 also had similar response to the flooded vegetation type (0.86 ± 0.52 and 0.73 µmol CO_2 m^{-2} s^{-1} for pasture, 1.01 ± 0.29 and 0.34 ± 0.06 µmol CO_2 m^{-2} s^{-1} for upland forest and 0.72 ± 0.37 and 0.62 ± 0.24 µmol CO_2 m^{-2} s^{-1} for seasonally flooded forest during high and low water, respectively).

As observed for pCO_2, there was no effect of reservoir type on FCO_2 variability during high water conditions ($F_{1:28}$= 0.32, R^2= 0.01, $p > 0.05$). In contrast, during low water conditions, FCO_2 varied significantly ($F_{1:17}$= 34.07, R^2= 0.61, $p < 0.05$), specifically in the IR, which had the highest average FCO_2 (0.69 ± 0.28 and 7.32 ± 4.06 µmol CO_2 m^{-2} s^{-1} for XR and IR, respectively). Fluxes of CO_2 in outside reservoir zones averaged 0.48 ± 0.61 µmol CO_2 m^{-2} s^{-1} and had a gradient pattern downstream. The furthest sites downstream of IR (90 and 25 km downstream

of the Belo Monte dam, respectively) had decreased average pCO_2 and FCO_2 values in relation to downstream of the dams' outflow (Table 2).

3.2 Gas transfer velocity (k_{600})

Gas transfer velocities were calculated for each chamber during the high and low water season of 2017. We were not able to estimate k for the 2016 high water season due to lack of pCO_2 measurements and as described for FCO_2 data, on k_{600} the spatial analysis also was made separately to each season due to different sensors used for flux measurements. The average k_{600} was 17.8 ± 10.2 and 34.1 ± 24.0 cm h^{-1} for high and low water seasons, respectively, without significant heterogeneity on the distribution through environments ($F_{2:9}$= 2.41, R^2= 0.46, p > 0.05 and $F_{2:12}$= 0.16, R^2= 0.03, p > 0.05, respectively). However, k_{600} had a strong pattern of correlation with wind velocities (r= 0.73; p < 0.05) during the high water season, although this pattern was not observed during the low water season (r= 0.53; p > 0.05).

Wind speeds ranged from 0.7 to 4.8 m s^{-1}, considering measurements for all sites and periods. However, no variation was observed between sampled seasons ($F_{1:37}$= 0.89, R^2= 0.01, p > 0.05). In contrast, there was significant variability of wind speeds among environments ($F_{2:37}$= 6.13, R^2= 0.23, p < 0.05) (Fig.5). Highest average wind speed was observed on the river channel while downstream of the dams had the lowest value (3.21 ± 0.89 and 1.66 ± 0.88 m s^{-1}, respectively) (Table 3).

3.3 Physical-chemical characteristics

The air temperatures at the studied sites varied between 27.5 and 33.8 °C during sampling in both seasons, with the maximum temperatures registered during the low water period. The superficial water temperature ranged from 29.2 to 32.7 °C, with maximum temperature registered during the high water period. The lowest and highest average pH values were observed in waters of flooded areas and river channel (Table 3). The water column was relatively well-oxygenated in all studied environments, reaching highest average DO concentration (7.28 ± 0.73 mg L^{-1}) in the outside reservoirs and lowest concentration in flooded areas (5.44 ± 2.00 mg L^{-1}) (Table 3). Conductivity varied from 18.40 to 38.30 µS cm^{-1} in the studied environments, with the highest average value (31.60 ± 8.63 µS cm^{-1}) in flooded areas and lowest (29.30 ± 4.85 µS cm^{-1}) downstream of the dams (Table 3).

In aquatic environments, CO_2 concentration is expected to correlate with physical-chemical characteristics of the water column. In the study sites, pCO_2 is negatively and strongly correlated with pH (r= -0.75; p < 0.05) and DO (r= -0.88; p < 0.05). Correlation between pCO_2 and water temperature was absent (p > 0.05) while FCO_2 was positively correlated with wind speed (r= 0.53; p < 0.05) (Figure 5) (Table 3).

4 Discussion

It has been shown that the amount of CO_2 in the water column and CO_2 emissions from Amazonian rivers to the atmosphere varies significantly among seasons, with higher fluxes generally observed during the high water season (Alin et al., 2011; Rasera et al., 2013; Richey et al., 2002; Sawakuchi et al., 2017). The increase in pCO_2 during the high water season can be related with the large input of terrestrial organic and inorganic carbon into the rivers by lateral surface and subsurface flow of water (Raymond and Saiers, 2010, Ward et al., 2017). In the study area, pCO_2 in areas flooded by reservoirs of the Belo Monte hydropower complex had higher average values than in the river channel even with the decrease from the high water to the low water season. Specifically

on the IR, there was an increase in pCO_2 during the low water season. Decaying vegetation and the carbon stored in the flooded soils may be the major and constant source of OM in flooded areas of hydropower reservoirs that stimulates heterotrophic activity and maintains a high and more stable CO_2 production during initial years of impoundment (Guérin et al., 2008). Consequently, pCO_2 in flooded areas of both XR and IR had little variation between the high and low water season due to constant renewal of OM and weak CO_2 sinks.

Another factor that may influence the seasonal variability in pCO_2 observed in the Xingu River is nutrient levels. In Amazonian lakes nitrogen and phosphorous normally have higher concentrations during the high water season, but become more available in the low water season due to the different vertical mixing pattern of each season (Tundisi et al.,1984). Higher concentrations of these nutrients would favor primary productivity (Farjalla et al., 2006; Vidal et al., 2015), taking up part of the CO_2 available in the water column. However, this algal biomass is readily consumed by heterotrophs (Qin et al., 2013), and in some cases stimulates the breakdown of terrestrially-derived OM (Ward et al., 2016). Thus, increased primary production may not always result in decreased pCO_2, per se.

The vertical heterogeneity of pCO_2 in the water column of the study site was registered by data acquired at three depth classes (surface, 60% and near bottom). The higher pCO_2 values observed in the near bottom can be attributed to an input of CO_2 from groundwater (Cole et al., 2007; Marotta et al., 2011) and from heterotrophic respiration in the sediments associated with a smaller uptake of CO_2 by photosynthetic activity by algae and macrophytes in the deeper layers of the water column than at the surface (Hansen and Blackburn, 1992). These processes can also vary according to different environmental conditions like water depth, allochthonous inputs and reservoir dimensions (Cardoso et al., 2013; Roland et al., 2010; Pacheco et al., 2015). Higher pCO_2 in the bottom waters was also related with lower dissolved oxygen and high pH, since heterotrophic respiration use O_2 and the increase in pCO_2 would lead to pH decrease due to the conversion of CO_2 into carbonic acid (H_2CO_3) (Duarte and Prairie, 2005; Frankignoulle et al., 1996; Neal et al., 1998; Wang et al., 2011).

Since pCO_2 and FCO_2 are intimately correlated, the pattern observed on pCO_2 extends to FCO_2. The high water FCO_2 and pCO_2 in the Belo Monte reservoirs area (Table 2) were in the same order of magnitude of emissions measured in Amazonian clearwater rivers unaffected by impoundment, including the Tapajós River, which has hydrologic conditions similar to the Xingu River (Alin et al., 2011; Rasera et al., 2013; Sawakuchi et al., 2017). Our low water average pCO_2 and FCO_2 values, however, had an opposite pattern in relation to literature values and were one order of magnitude higher (Table 2) than observed in clearwater rivers with natural flowing waters. Even when analyzed separately, the average FCO_2 values observed for the Belo Monte reservoirs (XR and IR) overcomes these natural emissions.

Large spatial heterogeneity was noticed in both Belo Monte reservoirs during high water season. The XR had main channel pCO_2 decreasing as FCO_2 increased and the contrary occurred in flooded areas, including the IR. The main carbon source of the XR is likely the standing vegetation (flooded forests and pasture), where higher pCO_2 for flooded areas was registered. Environmental conditions such as flooded vegetation play an important role in the CO_2 production, since it is the main source of OM for CO_2 production and may help to create gradients of reservoir CO_2 emissions (Roland et al., 2010; Teodoru et al., 2011). However, although with vegetation clearing, the most expressive emissions recorded in the study area are from the IR, where arboreal vegetation was suppressed before flooding, indicating that the OM in the flooded soil is a major source of carbon that is consumed and converted into CO_2. The diversity of environmental conditions in both Belo Monte reservoirs, like

vegetal suppression in IR, minor size of XR and consequently lesser flooded area, variation on hydrodynamic forces and water depth had significant influence on FCO_2 and pCO_2 values as occurs in other hydropower reservoirs (Cardoso et al. 2013; Teodoru et al., 2011, Räsänen et al., 2018; Roland et al., 2010).

About 42% of the XR area is the original channel of the Xingu River. However, the water velocity under reservoir conditions is slower than before since the water flow is regulated by Pimental dam spillways. FCO_2 measured upstream of the reservoir during the high water season, in a sector where the channel is flowing under natural conditions (Iriri river sites), was significantly higher than in the XR sector (Table 2). The increase of light penetration and nutrient supply combined with the decrease in water flow may favor primary productivity (Thomaz and Bini, 2007) as occurs in most hydropower reservoirs (McCartney, 2009; Ran et al., 2015; Zheng et al., 2011). Consequently, CO_2 concentrations in the water column may decrease, especially on upper layers, in response to the increased photosynthetic uptake of CO_2 during lower rainfall periods (Amaral et al., 2018). During the low water season, pCO_2 and FCO_2 drastically decreased, especially in the river channel. Contrary to high water, CO_2 fluxes were homogeneous and relatively low in most of the environments (with exception to IR) linked to elevated photosynthetic activity (Table 2). In addition, the CO_2 undersaturation in relation to atmosphere and negative fluxes is attributed to elevated primary productivity due to the high light penetrance, low suspended sediment concentration, which is similar to previously observations in Amazonian floodplain lakes and other clearwater rivers during the low water season (Amaral et al., 2018, Rasera et al 2013, Gagne-Maynard et al., 2017). The occurrence of negative CO_2 fluxes was observed only in outside reservoirs sectors, on furthest studied site downstream IR.

The IR is located on an upland forest area that received vegetation clearing before flooding. Even after the forest removal, the upper soil layer may have kept a high concentration of plant-derived material and it is still an important source of OM that may take several years to decay (Abril et al., 2005; Campo and Sancholuz, 1998; Guérin et al., 2006). This condition explains the higher average pCO_2 in IR than in XR, with the former area also having higher average FCO_2 values, possibly linked to wider open areas and a longer fetch for wind to create surface turbulence (Amaral et al., 2018; Paranaiba, et al. 2017). The XR has substrates with relatively reduced carbon storage because almost half of the area is represented by the original river channel dominated by bedrock or sandy substrates and flooding forest islands formed by sand and mud deposition, would not store much carbon (Sawakuchi et al., 2015).

Some differences emerge from the downstream emissions of the IR (5.26 $\pm$ 1.94 µmol CO_2 m^{-2} s^{-1} and 2,122 ± 106 µatm, to high water FCO_2 and pCO_2 respectively) and XR (2.85 ± 1.12 µmol CO_2 m^{-2} s^{-1} and 1,241 ± 48.24 µatm, to high water FCO_2 and pCO_2 respectively). In comparison to CO_2 emission of other downstream tropical storage reservoir, the FCO_2 of Petit Saut reservoir in French Guiana was almost double (10.49 ± 3.94 µmol CO_2 m^{-2} s^{-1}) (Guérin et al. 2006) of our highest downstream FCO_2 in IR during high water season. The FCO_2 in downstream zones of Belo Monte and Petit Saut reservoirs show CO_2 supersaturation similar to the reservoir waters. Although Petit Saut has a smaller dam and reservoir compared to the Belo Monte reservoirs, the elevated pCO_2 drove the downstream emissions. Both Belo Monte (this study) and Petit Saut (Guérin et al. 2006) reservoirs have waters most CO_2 supersaturated during the high water season. These CO_2 rich waters have potential to increase downstream emissions with the passage through the dam turbines as well as FCO_2 and pCO_2 may be altered for several km downstream the dam (Abril et al., 2005; Guérin et al., 2006; Kemenes et al., 2011; 2016).

In this study, the furthest downstream sites situated 90 and 25 km downstream the XR and IR, respectively, presented average pCO_2 and fluxes lower than the sites in the river channel upstream the XR. Our upstream XR sites also had higher FCO_2 than observed in undisturbed sectors of other large clearwater rivers in the Amazon (Table 2). The site downstream IR is within the river extent that could still be affected by the reservoir (Kemenes et al., 2016). However, the site further downstream the XR should be unaffected by the reservoir due to the long distance (90 km) and the fact that it receives waters from the Volta Grande region, where the bedrock riverbed with large rapids and waterfalls quickly degas the dissolved CO_2 coming from the upstream reservoir. Thus, this site could potentially be considered as a reference for natural FCO_2 values

The decrease in pCO_2 and FCO_2 persisted in areas downstream of the Belo Monte reservoirs as indicated by measurements performed during the high water and low water seasons. The higher FCO_2 and pCO_2 in the areas downstream of the dams of both reservoirs compared to river channel during high water indicates some turbine activity. However, this pattern is inconclusive at least for the low water season as the Belo Monte dam turbines were under installation and not fully operational. Therefore, downstream of both dams assumed river channel traits in relation to fluxes and CO_2 water saturation in this season.

Although no significant variation of k_{600} was observed between the reservoirs of the Belo Monte hydropower complex, the average values for high and low water were similar to observed values in other rivers of the Amazon Basin (Araguaia, Javaés, Tapajós and Teles Pires) (Alin et al. 2011; Rasera et al. 2013). We observed that in the XR reservoir area, FCO_2 values were higher in the main channel, where in addition to the constant water flow due to the ROR type reservoir, it also had a greater open area for wave formation in comparison with the sheltered flooded areas. This is consistent with the strong positive correlation observed between wind speed and FCO_2 here and in other large rivers where a vast water surface interacts with wind along its fetch, promoting the formation of waves that enhances water turbulence, k_{600} and FCO_2 (Abril et al., 2005; Paranaíba et al. 2017; Rasera et al., 2013; Raymond and Cole, 2001; Vachon et al., 2013).

Among the traits that differs for each hydropower dam, the operation design may play an important role for carbon fluxes in the reservoir and its downstream sector. In comparison to an older Amazonian reservoir with storage design, the Tucuruí reservoir built in 1984 in the clearwater Tocantins River presented CO_2 fluxes of 3.61 ± 1.62 µmol CO_2 m^{-2} s^{-1} (Lima et al., 2002), which is higher than fluxes observed in the XR, but it is three times lower than the highest flux registered for the IR in this study. The Tucuruí hydropower dam lacked vegetal suppression and has a large reservoir and hypolimnetical waters (Fearnside, 2002; Kemenes et al., 2016). Nevertheless, the Tucuruí CO_2 fluxes were measured 18 years after reservoir filling and estimates for storage reservoirs point out that 10 years after impounding, OM from flooded soils still contributes to carbon fluxes to the atmosphere (Abril et al., 2005; Guérin et al., 2008). Additionally, it must be considered that the Belo Monte hydropower complex had partial vegetation removal in some areas of the XR that potentially reduced observed CO_2 fluxes. Even with vegetal suppression, the IR emission is higher than other Amazonian dams, especially during low water conditions. Environmental and seasonal traits are important factors that influence CO_2 emissions, therefore it is important that reservoir type and dam design to maintain these conditions similar to natural river traits, in order to mitigate reservoir emissions.

5 Conclusions

Here we observed variability in CO_2 fluxes related to the type of environment and land use of flooded areas after impoundment of the Belo Monte hydropower complex. CO_2 emissions were 15 and 90% higher for the IR

compared to XR during high and low water season, respectively, indicating that storage reservoirs may be larger sources of CO_2 to the atmosphere compared to RORs. The Belo Monte hydropower complex had average CO_2 emission similar to Amazonian clearwater rivers without impounding in only one season (high water) and considerably lower than other tropical reservoirs. However, IR fluxes exceeded emissions measured in storage reservoirs of other tropical rivers. The IR presented the highest fluxes of the study even with vegetation removal. Although vegetation removal is perhaps one of the most effective approaches for reducing greenhouse gas emissions from hydropower reservoirs, we show that tropical reservoirs can present significant emissions even after vegetation suppression. Additional monitoring of CO_2 flux is needed to evaluate the Belo Monte hydroelectric complex emission with both dams working at full capacity, including measurements in the Volta Grande do Xingu region downstream the reservoir (XR) in the Xingu River channel. This is necessary to obtain robust and reliable assessment of carbon emissions related with the electricity produced by the Belo Monte hydropower complex over its entire lifecycle.

Author contribution

Kleiton R. Araújo collected and analyzed the data, as prepared the manuscript with contribution of all co-authors. Henrique O. Sawakuchi designed the study, cooperated in the field sampling and supported with guidance on data analysis. Dailson J. Bertassoli Jr. also collected the data and conducted the laboratorial analysis. André O. Sawakuchi attained the grant award, contributed to setting up the field equipment, measuring infrastructure and field sampling. Kleiton R. Araújo. Karina D. Silva and Thiago V. Bernardi conducted the statistical analysis. Nicholas D. Ward and Tatiana S. Pereira contributed with technical advice and guidance throughout the project implementation and paper writing stages.

Competing interests

We declare that we have no conflict of interests.

Acknowledgements

This study has funding by Fundação de Amparo à Pesquisa do Estado de São Paulo (FAPESP, grant 16/02656-9) and from Coordenação de Aperfeiçoamento de Pessoal de Nível Superior (CAPES) as master scholarship for Kleiton R. Araújo. We are grateful to Marcelo G. P. de Camargo, Hildegard de H. Silva, Victor A. T. Alem, Agna L. B. Figueiredo, and Thomas K. Akabame for the field sampling and laboratorial support. André O. Sawakuchi is supported by Conselho Nacional de Desenvolvimento Científico e Tecnológico (CNPq, grant 304727/2017-2).

References

Abril, G., Guérin, F., Richard, S., Delmas, R., Galy-Lacaux, C., Gosse, P., Tremblay, A., Varfalvy, L., Dos Santos, M. A. and Matvienko, B.: Carbon dioxide and methane emissions and the carbon budget of a 10-year old tropical reservoir (Petit Saut, French Guiana), Global Biogeochem. Cycles, 19, 1–16, doi:10.1029/2005GB002457, 2005.

Abril, G., Martinez, J.-M., Artigas, L. F., Moreira-Turcq, P., Benedetti, M. F., Vidal, L., Meziane, T., Kim, J.-H., Bernardes, M. C., Savoye, N., Deborde, J., Souza, E. L., Albéric, P., Landim de Souza, M. F. and Roland, F.: Amazon River carbon dioxide outgassing fuelled by wetlands, Nature, 505, 395–398, doi:10.1038/nature12797, 2014.

Alin, S. R., Rasera, M. D. F. F. L., Salimon, C. I., Richey, J. E., Holtgrieve, G. W., Krusche, A. V. and Snidvongs, A.: Physical controls on carbon dioxide transfer velocity and flux in low-gradient river systems and implications for regional carbon budgets, J. Geophys. Res. Biogeosciences, 116, doi:10.1029/2010JG001398, 2011.

Almeida, C. A., Coutinho, A. C., Esquerdo, J. C. D. M., Adami, M., Venturieri, A., Diniz, C. G., Dessay, N., Durieux, L., Gomes, A. R.: High spatial resolution land use and land cover mapping of the Brazilian Legal Amazon in 2008 using Landsat-5/TM and MODIS data. Acta Amaz. 46, 291–302. doi: 10.1590/1809-43922015 05504, 2016.

Amaral, J. H. F., Borges, A. V., Melack, J. M., Sarmento, H., Barbosa, P. M., Kasper, D., de Melo, M. L., De Fex-Wolf, D., da Silva, J. S. and Forsberg, B. R.: Influence of plankton metabolism and mixing depth on CO2 dynamics in an Amazon floodplain lake, Sci. Total Environ., 630, 1381–1393, doi:10.1016/j.scitotenv.2018.02.331, 2018.

ANA - Agência Nacional Das Águas. https:// http://www.snirh.gov.br/hidroweb/publico/medicoes_historicas_abas.jsf , last acess: 27 august 2017.

Anderson, M.J.: A new method for non-parametric multivariate analysis of variance. Austral Ecology, 26, 32-46, 2001.

Barros, N., Cole, J. J., Tranvik, L. J., Prairie, Y. T., Bastviken, D., Huszar, V. L. M., del Giorgio, P. and Roland, F.: Carbon emission from hydroelectric reservoirs linked to reservoir age and latitude, Nat. Geosci., 4, 593–596, doi:10.1038/ngeo1211, 2011.

Bastviken, D., Sundgren, I., Natchimuthu, S., Reyier, H. and Gålfalk, M.: Technical Note: Cost-efficient approaches to measure carbon dioxide (CO_2) fluxes and concentrations in terrestrial and aquatic environments using mini loggers, Biogeosciences, 12, 3849–3859, doi:10.5194/bg-12-3849-2015, 2015.

Battin, T. J., Kaplan, L. A., Findlay, S., Hopkinson, C. S., Marti, E., Packman, A. I., Newbold, J. D. and Sabater, F.: Biophysical controls on organic carbon fluxes in fluvial networks, Nat. Geosci., 2, 595–595, doi:10.1038/ngeo602, 2008.

Battin, T. J., Luyssaert, S., Kaplan, L. A., Aufdenkampe, A. K., Richter, A. and Tranvik, L. J.: The boundless carbon cycle, Nat. Geosci., 2, 598–600, doi:10.1038/ngeo618, 2009.

Brasil: Aproveitamento Hidrelétrico Belo Monte, Estudo de Impacto Ambiental, Eletrobrás, Rio de Janeiro, 36, 2009a.

Brasil: Aproveitamentos Hidrelétricos da Bacia Hidrográfica do Xingu, AAI - Avaliação Ambiental Integrada da Bacia do Rio Xingu, Eletrobrás, São Paulo, 204 pp., 2009b.

Brasil: Estudos para Licitação da Expansão da Geração AHE Belo Monte, Avaliação técnica, Empresa de Pesquisa Energética, Rio de janeiro, 87 pp., 2009c.

Brasil: Emissões de Gases de Efeito Estufa em Reservatórios de Centrais Hidrelétricas, Projeto BALCAR, Eletronorte, Rio de Janeiro, 400 pp., 2014.

Campo, J. and Sancholuz, L.: Biogeochemical impacts of submerging forests through large dams in the Rio Negro, Uruguay, J. Environ. Manage., 54, 59–66, doi:10.1006/jema.1998.0222, 1998.

Cardoso, S. J., Vidal, L. O., Mendonça, R. F., Tranvik, L. J., Sobek, S. and Roland F.: Spatial variation of sediment mineralization supports differential CO_2 emissions from a tropical hydroelectric reservoir, Front. Microbiol., 4, doi: 10.3389/fmicb.2013.00101, 2013.

Cole, J. J., Prairie, Y. T., Caraco, N. F., McDowell, W. H., Tranvik, L. J., Striegl, R. G., Duarte, C. M., Kortelainen, P., Downing, J. A., Middelburg, J. J. and Melack, J.: Plumbing the global carbon cycle: Integrating inland waters into the terrestrial carbon budget, Ecosystems, 10, 171–184, doi:10.1007/s10021-006-9013-8, 2007.

Csiki, S. and Rhoads, B. L.: Hydraulic and geomorphological effects of run-of-river dams, Prog. Phys. Geogr., 34, 755–780, doi:10.1177/0309133310369435, 2010.

Deemer, B. R., Harrison, J. A., Li, S., Beaulieu, J. J., Delsontro, T., Barros, N., Bezerra-Neto, J. F., Powers, S. M., Dos Santos, M. A. and Vonk, J. A.: Greenhouse gas emissions from reservoir water surfaces: A new global synthesis, Bioscience, 66, 949–964, doi:10.1093/biosci/biw117, 2016.

DelSontro, T., Perez, K. K., Sollberger, S. and Wehrli, B.: Methane dynamics downstream of a temperate run-of-the-river reservoir, Limnol. Oceanogr., 61, S188–S203, doi:10.1002/lno.10387, 2016.

Drake, T. W., Raymond, P. A. and Spencer, R. G. M.: Terrestrial carbon inputs to inland waters: A current synthesis of estimates and uncertainty, Limnol. Oceanogr. Lett., 3, doi:10.1002/lol2.10055, 2018.

Duarte, C. M. and Prairie, Y. T.: Prevalence of heterotrophy and atmospheric CO_2 emissions from aquatic ecosystems, Ecosystems, 8, 862–870, doi:10.1007/s10021-005-0177-4, 2005.

Egré, D. and Milewski, J. C.: The diversity of hydropower projects. Energy Policy, 30, 1225-1230, doi: 10.1016/S0301-4215(02)00083-6, 2002.

Faria, F. A. M., Jaramillo, P., Sawakuchi, H. O., Richey, J. E. and Barros, N.: Estimating greenhouse gas emissions from future Amazonian hydroelectric reservoirs, Environ. Res. Lett., 10, 124019, doi:10.1088/1748-9326/10/12/124019, 2015.

Farjalla, V. F., Azevedo, D. A., Esteves, F. A., Bozelli, R. L., Roland, F., Enrich-Prast, A.: Influence of hydrological pulse on bacterial growth and DOC uptake in a clear-water Amazonian lake. Microbial ecology, 52, 334-344, doi: 10.1007/s00248-006-9021-4, 2006.

Fearnside, P. M.: Greenhouse Gas Emissions from a Hydroelectric Reservoir (Brazil's Tucurui Dam) and the Energy Policy Impactions, 133, 69-96, doi: 10.1023/A:1012971715668, 2002.

Frankignoulle, M., Abril, G., Borges, A., Bourge, I., Canon, C., Delille, B., E., L. and Théare, J.: Carbon Dioxide Emission from European Estuaries, Science, 282, 434–436, doi:10.1126/science.282.5388.434, 1998.

Frankignoulle, M., Bourge, I. and Wollast, R.: Atmospheric CO_2, fluxes in a highly polluted estuary (the Scheldt), Limnol. Oceanogr., 41, 365-369, doi: 10.4319/lo.1996.41.2.0365, 1996.

Gagne-Maynard, W. C., Ward, N. D., Keil, R. G., Sawakuchi, H. O., Da Cunha, A. C., Neu, V., Brito, D. C., Less, D. F. S., Diniz, J. E. M., Valerio., A. M., Kampel, M., Krusche, A., V. and Richey, J. E.: Evaluation of primary production in the lower Amazon River based on a dissolved oxygen stable isotopic mass balance. Frontiers in Marine Science, 4, doi: 10.3389/fmars.2017.00026, 2017.

Guérin, F., Abril, G., Richard, S., Burban, B., Reynouard, C., Seyler, P. and Delmas, R.: Methane and carbon dioxide emissions from tropical reservoirs: Significance of downstream rivers, Geophys. Res. Lett., 33, 1–6, doi:10.1029/2006GL027929, 2006.

Guérin, F., Abril, G., de Junet, A. and Bonnet, M. P.: Anaerobic decomposition of tropical soils and plant material: Implication for the CO2 and CH4 budget of the Petit Saut Reservoir, Appl. Geochemistry, 23, 2272–2283, doi:10.1016/j.apgeochem.2008.04.001, 2008.

Hansen, L. S. and Blackburn, T. H.: Effect of algal bloom deposition on sediment respiration and fluxes. Marine Biology, 112, 147-152, doi: 10.1007/BF00349738, 1992.

Hesslein, R. H., Rudd, J. W. M., Kelly, C., Ramlal, P. and Hallard, K.: Carbon dioxide partial pressure in the surface waters of lakes in Northwestern, Ontario and the MacKenzie Delta region, Canada. in: Second International Symposium on Gas Transfer at Water Surfaces, Vicksburg, United States, August 1990, 413-431, 1991.

Inmet - Instituto Nacional De Meteorologia: https:// http://www.inmet.gov.br/projetos/rede/pesquisa/, last acess in: 12 july 2017.

Jähne, B. J., Münnich, K. O. M., Bösinger, R., Dutzi, A., Huber, W. and Libner, P.: On the Parameters Influencing Air-Water Gas Exchange, J. Geophys. Res., 92, 1937–1949, doi:10.1029/JC092iC02p01937, 1987.

Kemenes, A., Forsberg, B. R. and Melack, J. M.: CO_2 emissions from a tropical hydroelectric reservoir (Balbina, Brazil), J. Geophys. Res. Biogeosciences, 116, 1–11, doi:10.1029/2010JG001465, 2011.

Kemenes, A., Forsberg, B. R. and Melack, J. M.: Downstream emissions of CH_4 and CO_2 from hydroelectric reservoirs (Tucurui, Samuel, and Curua-Una) in the Amazon basin, Inl. Waters, 6, 295–302, doi:10.5268/IW-6.3.980, 2016.

Landchützer, P., Gruber, N., Bakker, D. C. E. and Schuster U.: Recent variability of glolbal ocean carbon sink, Global Biogeo. Cycles, 28, 927-949, doi: 10.1002/2014GB004853, 2014.

Latrubesse, E. M., Stevaux, J. C. and Sinha, R.: Tropical rivers, Geomorphology, 70, 187-206, doi: 10.1016/j.geomorph.2005.02.005, 2005.

Lima, I. B. T., Victoria, R. L., Novo, E. M. L. M., Feigl, B. J., Ballester, B. J and Ometto, J. P.: Methane, carbon dioxide and nitrous oxide emissions from two Amazonian Reservoirs during high water table, Verhandlungen, 28, 438-442, doi: 10.1080/03680770.2001.11902620, 2002.

Marotta, H., Duarte, C. M., Pinho, L., Enrich-Prast, A.: Rainfall leads to increased pCO_2 in Brazilian coastal lakes. Biogeosciences, 7, 1607-1614, doi:10.5194/bg-7-1607-2010, 2011.

McCartney, M.: Living with dams: Managing the environmental impacts, Water Policy, 11, 121–139, doi:10.2166/wp.2009.108, 2009.

Neal, C., House, W. A., Jarvie, H. P. and Eatherall, P.: The significance of dissolved carbon dioxide in major lowland rivers entering the North Sea, Sci. of the Tot. Env., 210, 187-203, doi: 10.1016/j.scitotenv.2016.08.201, 1998.

Oksanen, J., Blanchet, F. G., Friendly, M., Kindt, R., Legendre, P., McGlinn, D., Michin, P. R.,O'Hara, R. B., Simpson, G. L., Solymos, P., Stevens, M. H. H., Szoecs, E. and Wagner, H.: vegan: Community Ecology Package. R package version 2. 4-3. 2017.

Pacheco, F. S., Soares, M. C. S., Assireu, A. T., Curtarelli, A. T., Roland, F., Abril, G., Stech, J. L., Alvalá, P. C. and Ometto, J. P.: The effects of river inflow and retention time on the spatial heterogeneity of chlorophyll and water–air CO2 fluxes in a tropical hydropower reservoir, Biogeosciences, 12, 147-162, doi: 10.5194/bg-12-147-2015, 2015.

Paranaíba, J. R., Barros, N., Mendonça, R., Linkhorst, A., Isidorova, A., Roland, F., Almeida, R. M. and Sobek, S.: Spatially resolved measurements of CO2 and CH4 concentration and gas-exchange velocity highly influence carbon-emission estimates of reservoirs, Environ. Sci. Technol., 52, 607–615, doi:10.1021/acs.est.7b05138, 2018.

Qin, B., Gao, G., Zhu, G., Zhang, Y., Song, Y., Tang, X., Xu, H., Deng, J.: Lake eutrophication and its ecosystem response. Chinese Science Bulletin, 58, 961-970, doi: 10.1007/s11434-012-5560-x, 2013.

R Core Team. R: A Language and Environment for Statistical Computing. R Foundation for Statistical Computing, Vienna, Austria. 2016.

Ran, L., Lu, X. X., Richey, J. E., Sun, H., Han, J., Yu, R., Lao, S. and Yi, Q.: Long-term spatial and temporal variation of CO_2 partial pressure

in the Yellow River, China, Biogeosciences, 12, 921-934, doi:10.5194/bg-12-921-2015, 2015.

Räsänen, T. A., Varis, O., Scherer, L. and Kummu, M.: Greenhouse gas emissions of hydropower in the Mekong River Basin, Environ. Res. Lett., 13, 34030, doi:10.1088/1748-9326/aaa817, 2018.

Rasera, M. de F. F. L., Krusche, A. V., Richey, J. E., Ballester, M. V. R. and Victória, R. L.: Spatial and temporal variability of pCO_2 and CO_2 efflux in seven Amazonian Rivers, Biogeochemistry, 116, 241–259, doi:10.1007/s10533-013-9854-0, 2013.

Raymond, P. A. and Cole, J. J.: Gas Exchange in Rivers and Estuaries: Choosing a Gas Transfer Velocity, Estuaries, 24, 312, doi:10.2307/1352954, 2001.

Raymond, P. A. and Saiers, J. E.: Event controlled DOC export from forested watersheds, Biogeochemistry, 100, 197–209, doi:10.1007/s10533-010-9416-7, 2010.

Raymond, P. A., Hartmann, J., Lauerwald, R., Sobek, S., McDonald, C., Hoover, M., Butman, D., Striegl, R., Mayorga, E., Humborg, C., Kortelainen, P., Dürr, H., Meybeck, M., Ciais, P. and Guth, P.: Global carbon dioxide emissions from inland waters, Nature, 503, 355–359, doi:10.1038/nature12760, 2013.

Richey, J. E., Melack, J. M., Aufdenkampe, A. K., Ballester, V. M. and Hess, L. L.: Outgassing from Amazonian rivers and wetlands as a large tropical source of atmospheric CO2. Nature, 416, doi: 10.1038/416617a, 2002.

Roland, F., Vidal, L. O., Pacheco, F. S., Barros, N. O., Assireu, A., Ometto, J. P. H. B., Cimbleris, A. C. P. and Cole, J. J.: Variability of carbon dioxide flux from tropical (Cerrado) hydroelectric reservoirs, Aquat. Sci., 72, 283–293, doi:10.1007/s00027-010-0140-0, 2010.

Sawakuchi, A. O., Hartmann, G. A., Sawakuchi, H. O., Pupim, F. D. N., Bertassoli, D. J., Parra, M., J. L. Antinao, L. M. Sousa, M. H. Sabaj Pérez, P. E. Oliveira, R. A Santos, J. F. Savian, C. H. Grohmann, V. B. Medeiros, M. M. McGlue, D. C. Bicudo, and S. B. Faustino.: The Volta Grande do Xingu: reconstruction of past environments and forecasting of future scenarios of a unique Amazonian fluvial landscape. Scientific Drilling, 20, doi: 10.5194/sd-20-21-2015, 2015.

Sawakuchi, H. O., Neu, V., Ward, N. D., Barros, M. de L. C., Valerio, A. M., Gagne-Maynard, W., Cunha, A. C., Less, D. F. S., Diniz, J. E. M., Brito, D. C., Krusche, A. V. and Richey, J. E.: Carbon Dioxide Emissions along the Lower Amazon River, Front. Mar. Sci., 4, 1–12, doi:10.3389/fmars.2017.00076, 2017.

Sioli, H.,: The Amazon and its main affluents: Hidrology, morpholy of the river courses and river types, in: The Amazon : limnology and landscape ecology of a mighty tropical river and its basin, Dr W. Junk Publishers, Netherlands, edited by: Sioli, H. and Dumont, H. J., 127 – 165, doi: 10.1007/978-94-009-6542-3, 1984.

St. Louis, V. L., Kelly, C. A., Duchemin, E., Rudd, J. W. M. and Rosenberg D. M.: Reservoir surfaces as sources of greenhouse gases to the atmosphere: a global estimate, BioScience, 5, 766-775, doi: 10.1641/0006-3568(2000)050[0766:RSASOG]2.0.CO;2, 2000.

Teodoru, C. R., Prairie, Y. T. and Del Giorgio, P. A.: Spatial Heterogeneity of Surface CO2 Fluxes in a Newly Created Eastmain-1 Reservoir in Northern Quebec, Canada, Ecosystems, 14, 28–46, doi:10.1007/s10021-010-9393-7, 2011.

Thomaz, S. M. and Bini, L. M.: Expansão das Macrófitas Aquáticas e Implicações para o Manejo de Reservatórios: Um Estudo na Represa de Itaipu. In: Ecologia de Reservatórios: Estrutura, Função e Aspectos Sociais, edited by: Henry, R., Botucatu, Fundibio, 597 - 626, 2007.

Tundisi, J. G., Forsberg, B. R., Devol, A. H., Zaret, T. M., Tundisi, T. M., Dos Santos, A., Ribeiro, J. S. and Hardy, E. R.: Mixing patterns in Amazon lakes. Hydrobiologia, 108, 3-15, doi: 10.1007/BF02391627, 1984.

Vachon, D., Prairie, Y. T. and Smith, R.: The ecosystem size and shape dependence of gas transfer velocity versus wind speed relationships in lakes, Can. J. Fish. Aquat. Sci., 70, 1757–1764, doi:10.1139/cjfas-2013-0241, 2013.

Vidal, L. O., Abril, G., Artigas, L. F., Melo, M. L., Bernardes, M. C., Lobão, L. M., Rei, M. C., Moreira-Turcq, P., Benedetti, M., Tornisielo, V. L., Roland, F.: Hydrological pulse regulating the bacterial heterotrophic metabolism between Amazonian mainstems and floodplain lakes. Frontiers in microbiology, 6, 1054. doi: 10.3389/fmicb.2015.01054, 2015.

Wang, F., Wang, B., Liu, C. Q., Wang, Y., Guan, J., Liu, X. and Yu, Y.: Carbon dioxide emission from surface water in cascade reservoirs-river system on the Maotiao River, southwest of China, Atmos. Environ., 45, 3827–3834, doi:10.1016/j.atmosenv.2011.04.014, 2011.

Wanninkhof, R., Asher, W. E., Ho, D. T., Sweeney, C. and McGillis, W. R.: Advances in Quantifying Air-Sea Gas Exchange and Environmental Forcing, Ann. Rev. Mar. Sci., 1, 213–244, doi:10.1146/annurev.marine.010908.163742, 2009.

Wanninkhof, R. H.: Relationship between wind speed and gas exchange, J. Geophys. Res., 97, 7373–7382, doi:10.1029/92JC00188, 1992.

Ward, N. D., Keil, R. G., Medeiros, P. M., Brito, D. C., Cunha, A. C., Dittmar, T., Yager, P. L., Krusche, A. V. and Richey, J. E.: Degradation of terrestrially derived macromolecules in the Amazon River, Nat. Geosci., 6, 530–533, doi:10.1038/ngeo1817, 2013.

Ward, N. D., Bianchi, T.S., Sawakuchi, H.O., Gagne-Maynard, W., Cunha, A.C., Brito, D.C., Neu, V., Matos Valerio, A., Silva, R., Krusche, A.V. and Richey, J. E.: The reactivity of plant-derived organic matter and the potential importance of priming effects along the lower Amazon River. Journal of Geophysical Research: Biogeosciences, 121, 1522-1539, doi: 10.1002/2016JG003342, 2016.

Ward, N. D., Bianchi, T.S., Medeiros, P. M., Seidel, M., Richey, J. E., Keil, R. G. and Sawakuchi, H. O.: Where carbon goes when water flows: carbon cycling across the aquatic continuum. Frontiers in Marine Science, 4, doi: 10.3389/fmars.2017.00007, 2017.

Wiesenburg, D. A. and Guinasso Jr, N. L.: Equilibrium solubilities of methane, carbon monoxide, and hydrogen in water and sea water. Journal of chemical and engineering data, 24, 356-360, doi:10.1021/je60083a006, 1979.

Winemiller, K. O., McIntyre, P. B., Castello, L., Fluet-Chouinard, E., Giarrizzo, T., Nam, S., Baird, I. G., Darwall, W., Lujan, N. K., Harrison, I.,

Stiassny, M. L. J., Silvano, R. A. M., Fitzgerald, D. B., Pelicice, F. M., Agostinho, A. A., Gomes, L. C., Albert, J. S., Baran, E., Petrere, M., Zarfl, C., Mulligan, M., Sullivan, J. P., Arantes, C. C., Sousa, L. M., Koning, A. A., Hoeinghaus, D. J., Sabaj, M., Lundberg, J. G., Armbruster, J., Thieme, M. L., Petry, P., Zuanon, J., Vilara, G. T., Snoeks, J., Ou, C., Rainboth, W., Pavanelli, C. S., Akama, A., van Soesbergen, A. and Saenz, L.: Balancing hydropower and biodiversity in the Amazon, Congo, and Mekong, Science, 351, 128–129, doi:10.1126/science.aac7082, 2016.

Zar, J. H.: Biostatistical Analysis, 5° Ed., Pearson, New Jersey, 931 pp., 2010.

Zheng, T. G., Mao, J. Q., Dai, H. C. and Liu, D. F.: Impacts of water release operations on algal blooms in a tributary bay of Three Gorges Reservoir, Sci. China Technol. Sci., 54, 1588–1598, doi:10.1007/s11431-011-4371-7, 2011.

Figure captions

Fig.1: Average river discharge (in $m^3 s^{-1}$) of the Xingu River (left Y axis) and precipitation (in mm $month^{-1}$) (right Y axis) at Altamira from 2004 to 2014. Bars indicate monthly standard deviation. Data is from ANA (2017) and Inmet (2017).

Fig.2: Sampling sites upstream (Iriri river), within and downstream of the reservoirs and the location of the two dams (white bars) in the Xingu river. Land cover data is based on vegetation characterization from Almeida et al. (2016), here non-forested area groups pasture, deforested, secondary vegetation and urban areas.

Fig.3: Boxplots showing the spatial and temporal variability of pCO_2 and FCO_2. Whiskers indicate standard deviation, boxes are maximum and minimum values and the middle points are mean values. High water FCO_2 (2016 and 2017 campaigns) and pCO_2 from all depths values were averaged to characterize the environmental category. Temporal variation may be observed by the overall seasonal variation to pCO_2 and FCO_2 during high (A) and low water (B), likewise the spatial distribution to both pCO_2 (C) and FCO_2 (D) on each season and according environment.

Fig.4: Spatial and temporal variation of the FCO_2 values (µmol CO_2 m^{-2} d^{-1}) in the reservoirs (XR and IR) of the Belo Monte hydropower complex during high water (A) and low water (B) seasons. High water season data include both averages of measurements carried out during the years of 2016 and 2017. Colors and circles sizes indicate type and intensity of CO_2 fluxes.

Fig.5: Scatterplots between FCO_2 (A) and k_{600} (B) as a function of wind speed. Values from figure 5 (A) include high and low water seasons. Figure 5 (B) comprises only high water values for statistical correlation (Spearman correlation).

Biogeosciences Discuss., https://doi.org/10.5194/bg-2019-53
Manuscript under review for journal Biogeosciences
Discussion started: 18 February 2019

Figures

Fig.1

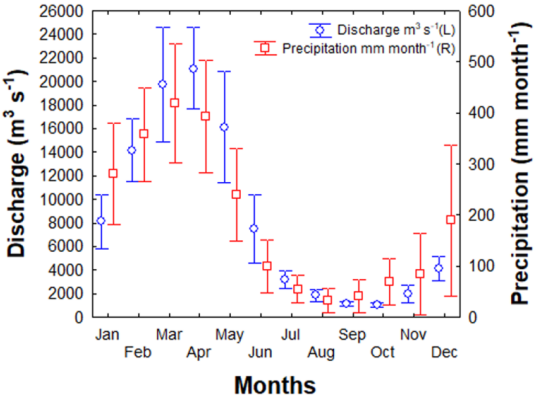

Fig.2

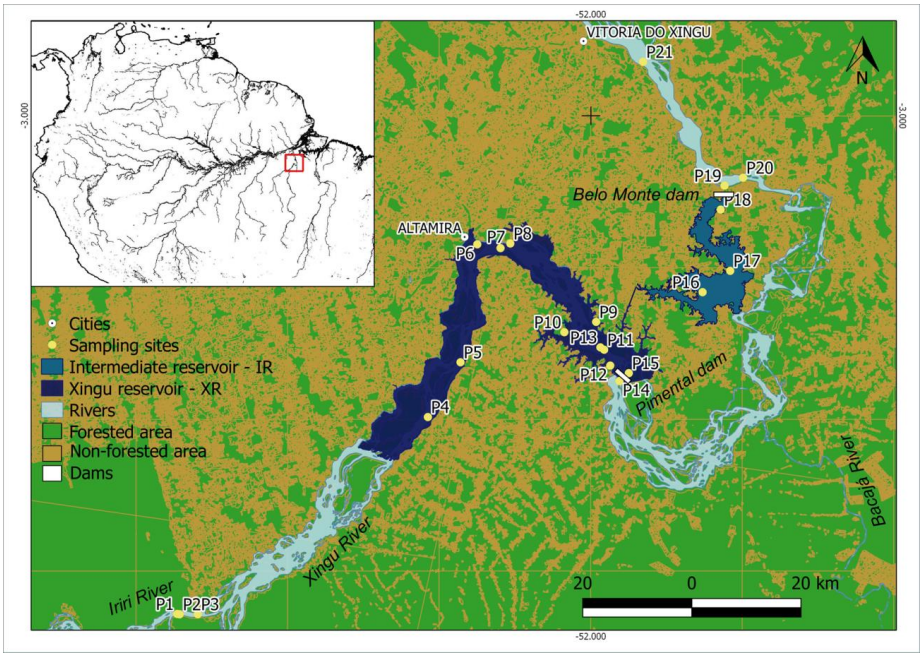

Biogeosciences Discuss., https://doi.org/10.5194/bg-2019-53
Manuscript under review for journal Biogeosciences
Discussion started: 18 February 2019

Fig.3

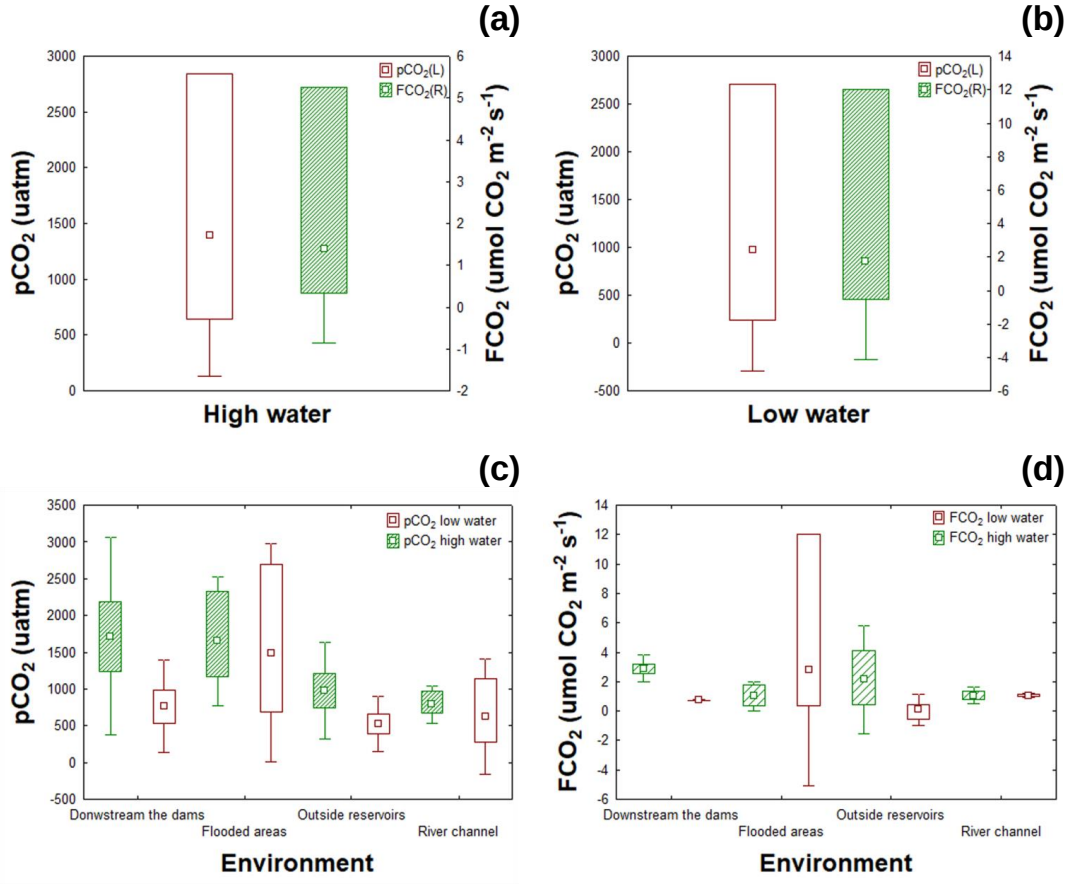

Biogeosciences Discuss., https://doi.org/10.5194/bg-2019-53
Manuscript under review for journal Biogeosciences
Discussion started: 18 February 2019

740 Fig.4

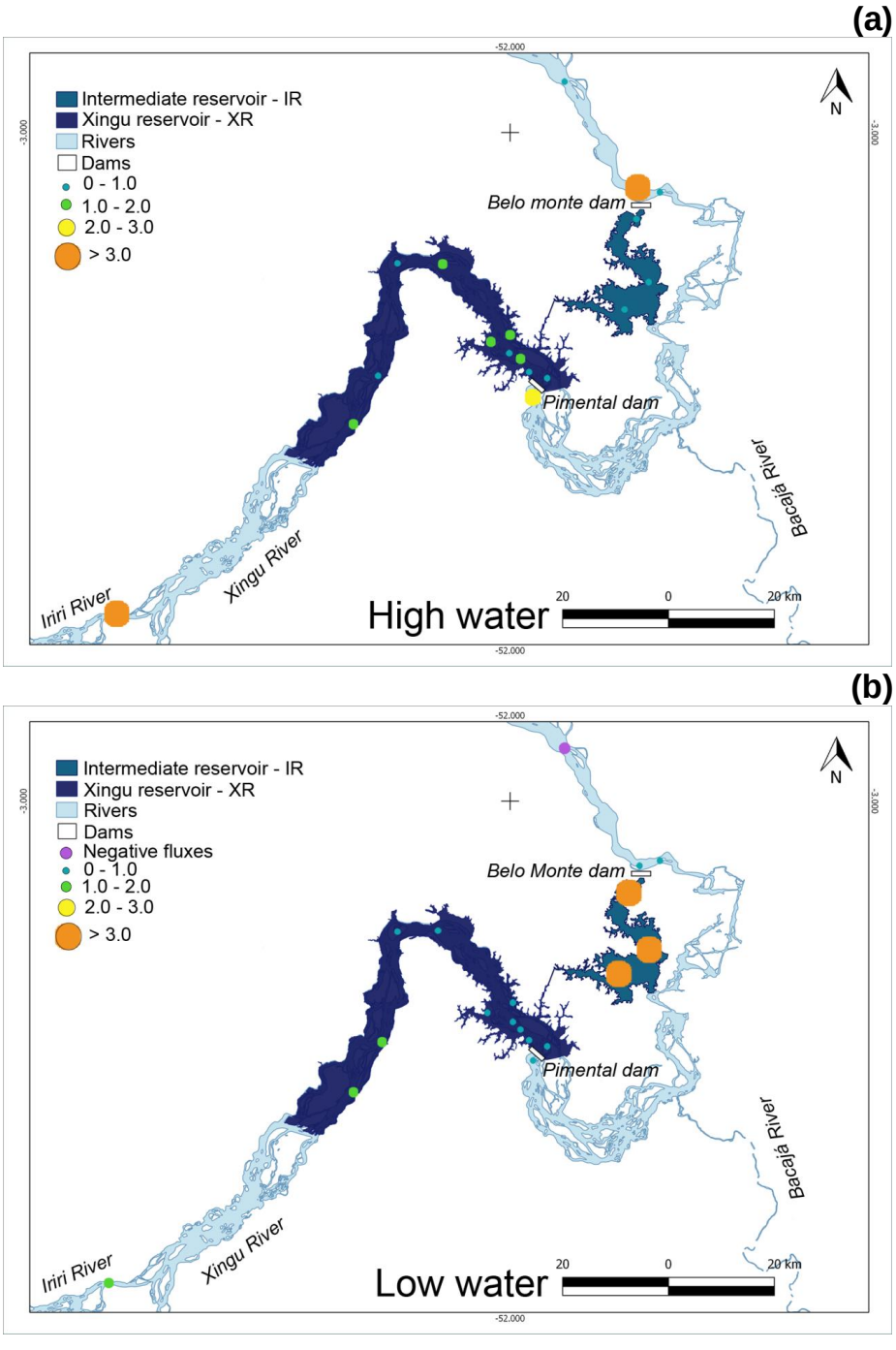

745

Biogeosciences Discuss., https://doi.org/10.5194/bg-2019-53
Manuscript under review for journal Biogeosciences
Discussion started: 18 February 2019

Fig.5:

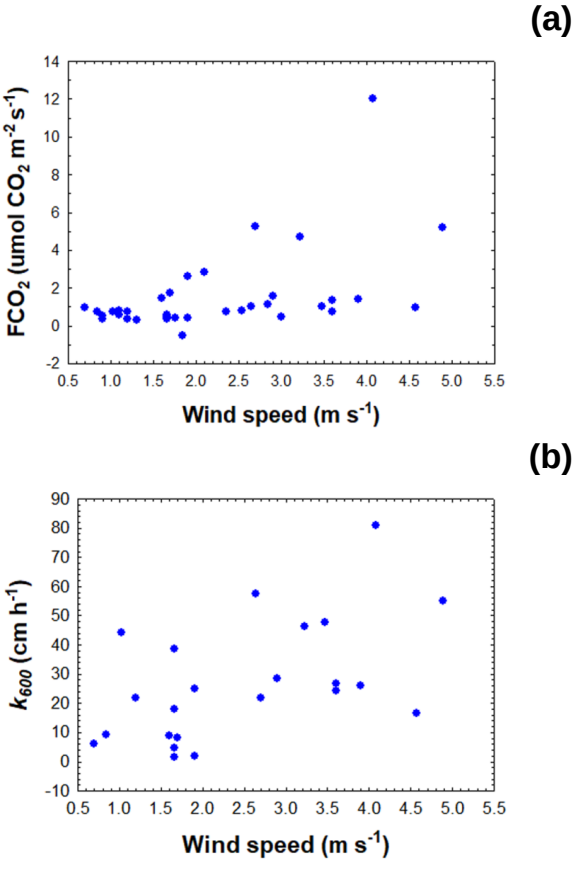

Table captions

Table 1: Locations of sampling sites in the Xingu and Iriri Rivers and reservoirs (XR and IR) of the Belo Monte hydropower complex. Sites were classified according to pre and post-flooded vegetation types, water depth and sampling season (H1: high water of 2016, H2: high water of 2017 and L: low water of 2017).

Table 2: Summary of FCO_2, pCO_2, gas transfer velocities (k_{600}) averages and literature values. High water season averages to FCO_2 comprehends both sampling years, since no significant variation was detected. FCO_2, pCO_2 and k_{600} referential values (FCO_2 Lit, pCO_2 Lit and k_{600} Lit, respectively) were averaged from the Amazonian clear water rivers Tapajós (Alin et al. 2011 and Sawakuchi et al. 2017), Araguaia, Javaés and Teles Pires (Rasera et al. 2013) in the correspondent season when available.

Table 3: Overall average values for physical-chemical conditions comprising the three depth classes (surface, 60% and near bottom) sampled during the high water seasons of 2016 and 2017, with exception to Temp (water temperature) and WS (wind speed), which corresponds to both high and low water. The variables pH (hydrogen potential), DO (dissolved oxygen), Cond (conductivity), Temp and WS are presented according to environment.

Biogeosciences Discuss., https://doi.org/10.5194/bg-2019-53
Manuscript under review for journal Biogeosciences
Discussion started: 18 February 2019

Tables

Table 1

Site	Longitude	Latitude	Pre-flooding environment	Season	Depth (m)
P1	-3.82115	-52.682559	River channel	H1	ND
P2	-3.82168	-52.678553	River channel	L	13.0
P3	-3.82153	-52.678599	River channel	L	8.0
P4	-3.49656	-52.268961	River channel	H2, L	8.1
P5	-3.40623	-52.215154	River channel	H2, L	7.5
P6	-3.21182	-52.187488	Seasonally flooded forested island	H1, H2, L	3.0
P7	-3.21801	-52.149169	River channel	H1, H2, L	20.5
P8	-3.21045	-52.133034	Pasture*	H1, H2, L	0.35
P9	-3.33965	-51.991423	Upland forest*	H1, H2, L	6.1
P10	-3.35664	-52.043752	Tributary, reservoir	H2, L	5.1
P11	-3.38557	-51.978184	River channel	H1, H2, L	19.3
P12	-3.41172	-51.968102	Pasture*	H1, H2, L	6.0
P13	-3.38170	-51.984364	Seasonally flooded* forest	H2, L	7.4
P14	-3.38557	-51.978184	River channel	H1, H2, L	2.5
P15	-3.42413	-51.937447	Seasonally flooded forested island	H1, H2, L	11.0
P16	-3.29069	-51.815787	Upland forest	H2, L	20.4
P17	-3.44253	-51.954685	Upland forest	H2, L	6.2
P18	-3.15452	-51.785845	Upland forest	H2, L	58.3
P19	-3.11501	-51.779624	River channel	H1, H2, L	6.2
P20	-3.10197	-51.748847	River channel	H2, L	2.6
P21	-2.91097	-51.913989	River channel	H1, H2, L	9.0

ND - No data collected.
**vegetation not removed prior to reservoirs filling.*

Biogeosciences Discuss., https://doi.org/10.5194/bg-2019-53
Manuscript under review for journal Biogeosciences
Discussion started: 18 February 2019

Table 2

Environment	Reservoir	Sampling season	FCO_2 (µmol CO_2 m^{-2} s^{-1})	pCO_2 (µatm)			k_{600} (cm h^{-1})	FCO_2 Lit (µmol CO_2 m^{-2} s^{-1})		pCO_2 Lit (µatm)		k_{600} Lit (cm h^{-1})		References
				Surface	60%	Near bottom		High water	Low water	High water	Low water	High water	Low water	
Upstream	OR	High	4.10 ± 2.16	ND	ND	ND	ND	ND	0.75 ± 0.41	ND	643 ± 172	ND	16.87 ± 10.36	Alin et al. 2011
		Low	1.06	501 ± 71.32	ND	766 ± 138	47.94							
River channel	XR	High	1.27 ± 0.31	771 ± 56.20	ND	808 ± 205	26.58 ± 2.10							
		Low	0.89 ± 0.33	612 ± 161	281 ± 143	871 ± 783	30.70 ± 24.64							
Flooded areas	XR	High	0.78 ± 0.38	1,674 ± 17.80	1,647 ± 333	2,838 ± 83.19	8.91 ± 3.22	2.6 ± 1.12	-0.06 ± 0.15	1,646 ± 663	377 ± 154	11.70 ± 5.45	5.17 ± 3.39	
		Low	0.47 ± 0.12	1,330 ± 1,210	807 ± 103	1,498 ± 203	15.07 ± 20.49							
Flooded areas	IR	High	1.08 ± 0.62	1,556 ± 375	1,876 ± 37.48	1,696 ± 455	7.13 ± 1.59	2.3 ± 0.41	0.4 ± 0.18	2,620 ± 810	724 ± 334	8.22 ± 3.80	5.05 ± 0.77	Rasera et al. 2013
		Low	7.32 ± 4.07	1,526 ± 263	ND	2,069 ± 152	60.80 ± 18.02							
Downstream the dams	OR	High	2.89 ± 1.74	2,122 ± 106	1,729 ± 689	2,257 ± 42.23	21.86 ± 11.01	1.92 ± 0.96	0.4 ± 0.15	1,799 ± 753	1,037 ± 635	12.20 ± 4.35	7.0 ± 6.64	
		Low	0.75 ± 0.01	663 ± 372	ND	861 ± 257	26.90 ± 24.69							
Further downstream	OR	High	1.55 ± 1.08	969 ± 341	ND	998 ± 316	13.61 ± 16.33	1.75	0.76	450	449	ND	16.03	Sawakuchi et al. 2017
		Low	-0.07 ± 0.62	409 ± 137	ND	650 ± 239	34.86 ± 18.49							
Overall average		**High**	**1.38 ± 1.12**	**1,193 ± 520**	**1,618 ± 525**	**1,372 ± 755**	**15.61 ± 8.36**							
		Low	**1.74 ± 2.94**	**877 ± 651**	**676 ± 276**	**1,191 ± 654**	**34.39 ± 17.74**							

IR – Intermediate reservoir.

ND - No data available.

OR - outside reservoir.

XR - Xingu reservoir.

Biogeosciences Discuss., https://doi.org/10.5194/bg-2019-53
Manuscript under review for journal Biogeosciences
Discussion started: 18 February 2019

Table 3

Environment	pH	DO (mg L^{-1})	Cond (µS cm^{-1})	Temp (°C)	WS (m s^{-1})
Downstream of dams	6.62 ± 0.18	5.87 ± 1.39	29.30 ± 4.85	29.52 ± 0.09	1.66 ± 0.88
Flooded areas	6.60 ± 0.26	5.44 ± 2.00	31.60 ± 8.63	29.85 ± 0.66	1.96 ± 1.13
Outside Reservoirs	6.75 ± 0.24	7.28 ± 0.73	30.59 ± 6.87	29.72 ± 0.36	2.06 ± 0.84
River channel	6.81 ± 0.21	6.92 ± 0.26	29.86 ± 5.30	29.44 ± 0.62	3.21 ± 0.89